JGR Oceans

RESEARCH ARTICLE
10.1029/2019JC015789

Special Section:
Contributions from the Physics of Estuaries and Coastal Seas meeting, 2018

Inversions of Estuarine Circulation Are Frequent in a Weakly Tidal Estuary With Variable Wind Forcing and Seaward Salinity Fluctuations

Xaver Lange[1], Knut Klingbeil[1], and Hans Burchard[1]

[1]Leibniz Institute for Baltic Sea Research Warnemünde (IOW), Rostock, Germany

Key Point:
- The circulation in weakly tidal estuaries is strongly influenced by wind straining and buoyancy gradient forcing and can be reversed

Correspondence to:
X. Lange,
xaver.lange@io-warnemuende.de

Citation:
Lange, X., Klingbeil, K., & Burchard, H. (2020). Inversions of estuarine circulation are frequent in a weakly tidal estuary with variable wind forcing and seaward salinity fluctuations. *Journal of Geophysical Research: Oceans*, *125*, e2019JC015789. https://doi.org/10.1029/2019JC015789

Received 19 DEC 2019
Accepted 13 MAY 2020
Accepted article online 15 JUN 2020

[Correction added on 4 SEP 2020, after first online publication: Projekt Deal funding statement has been added.]

Abstract The hydrodynamics in estuaries is mainly governed by the competition between a horizontal density gradient, friction, and wind stress. The sensitivity of the estuarine exchange flow to the wind stress increases in the absence of tides, which is investigated here using the example of the weakly tidal Warnow river estuary in the southwestern Baltic Sea—the mouth of which is characterized by strongly varying salinities of 8 to 20 g kg^{-1}. The interaction between a volatile salinity gradient and along-estuary wind forcing is found to cause temporary inversions of the estuarine circulation. Despite the highly dynamic conditions, the applicability of recent theories for isohaline mixing, using the framework of Total Exchange Flow, and the strength of the exchange flow, using a non-dimensional parameter space, could be confirmed. By analyzing salinity fluxes at the mouth of the estuary, a mixing completeness of 84% was calculated for the estuary. Furthermore, inversion of estuarine circulation was typically found for a local Wedderburn number (ratio of non-dimensional wind stress to non-dimensional horizontal density gradient) exceeding 0.33, indicating a high sensitivity to along-estuary wind.

Plain Language Summary Physics in estuary systems is mainly controlled by friction, wind, and the salinity difference between the coastal sea and the river. The importance of wind increases when the tidal range is small. This is investigated here at the weakly tidal Warnow estuary in the southwestern Baltic Sea, which is characterized by a strongly varying salinity. Both the wind and the salinity gradient reverse the direction of the exchange flow if a critical threshold value is exceeded.

1. Introduction

Estuaries are complex coastal systems that can be found all over the world and differ in numerous aspects, such as bio-geo-chemistry, morphology, and physics. Focusing on the latter, Wang et al. (2017) recently described an estuary as "a mixing machine that combines high salinity water from the ocean with fresh water from the river to form intermediate-salinity water." Classical (or positive) estuaries have in common that a net near-bottom landward inflow transports seawater into the estuary which is then transformed by estuarine processes (e.g., mixing) into a net near-surface seaward directed outflow, when averaged over a certain period of time. This bidirectional exchange flow, also referred to as estuarine circulation, is a key mechanism in estuarine dynamics (Geyer & MacCready, 2014; MacCready & Geyer, 2010). Earliest studies identified the longitudinal density gradient, resulting from the salinity difference between seawater and riverine water, as the major driver for this process (Chatwin, 1976; Hansen & Rattray, 1965; Pritchard, 1952, 1954, 1956), motivating a more precise phrasing of this type of exchange flow as gravitational circulation. In contrast to a positive circulation, inverse (or negative) estuaries are identified by a net near-surface landward transport of volume in combination with a compensating net outflow near the bottom pointing seaward. Negative estuaries, as those existing, for example, in arid regions characterized by strong evaporation, have a reversed longitudinal salinity gradient as, for example, the Persian Gulf (Johns et al., 2003) or the Spencer Gulf in south Australia (Nunes & Lennon, 1986). Temporary inverted circulation in classical estuaries can also be observed in the presence of strong landward wind (Lange & Burchard, 2019; Scully et al., 2005). Observations by Scully et al. (2005) in the York River estuary showed a strong correlation between the exchange flow and the longitudinal wind, with seaward wind increasing estuarine circulation (and stratification) and landward wind decreasing the exchange flow. Chen and Sanford (2009) investigated this competition between wind straining and wind mixing using a bulk formulation of the Wedderburn number (ratio of wind stress to density gradient). They showed in a set of numerical simulations that the

latter controls the effectiveness of wind straining, with up-estuary wind stress decreasing stratification and down-estuary winds being able to increase or decrease stratification depending on their strength.

Based on a set of non-dimensional parameters, Lange and Burchard (2019) studied the influence of up- and down-estuary wind forcing on either supporting or opposing gravitationally driven estuarine circulation. They showed that the circulation reverses its direction when the ratio of local non-dimensional wind stress to local non-dimensional density gradient exceeds a critical value. Through the use of a series of parameter studies, it was found that the latter, introduced as the basic Wedderburn number, is largely independent of the state of an estuary but rather describes the sensitivity of a system to wind stress itself. Its value ranges from 0.15 (stationary analytical solution), over 0.45 (including tidal straining), up to 1.3 (additionally including lateral effects), pointing out that the more processes are involved in driving classical estuarine circulation, the more up-estuary wind forcing is needed to invert the circulation direction. Applied to a realistic tidal inlet in the Wadden Sea in the southeastern North Sea, the basic Wedderburn number yielded a value of We_b=0.6, which indicates a reversal if the non-dimensional wind stress is greater than 60% of the non-dimensional longitudinal density gradient. In addition to strong up-estuary wind forcing, a rapidly decreasing coastal salinity has been observed to reverse the exchange flow temporary (see, e.g., Flöser et al., 2011). This is the case when the adaptation time of the estuary to the outer salinity is slower than the outer changes and the salinity stored in the estuary is larger than in the coastal water.

In order to quantify mixing in estuaries, different approaches have been suggested in the past. Aside from using the eddy diffusivity as a measure for tidal mixing (e.g., Hansen & Rattray, 1965; Hetland & Geyer, 2004), a quantification in terms of the dissipation of salinity variance (Burchard & Rennau, 2008) drew some attention recently. Wang et al. (2017) applied the latter in order to study volume-integrated mixing in the Hudson River estuary using a numerical model and the isohaline Total Exchange Flow (TEF) framework (MacCready, 2011), for describing transports of volume and salt. Using TEF and a salinity variance budget, MacCready et al. (2018) showed that the total system-wide mixing in an estuary can be estimated as the simple product of inflow salinity, outflow salinity, and freshwater discharge when considering long-term averages. Based on this, Burchard et al. (2019) derived a more detailed formulation by allowing additionally non-constancy of salinity and including the effect of storage of volume and salt.

Thus, the estuarine exchange flow and its related salt fluxes and volume transports are dependent on the amount of freshwater discharge, mixing and stratification, local tidal characteristics, and the prevailing buoyancy gradient and wind stress. Note that apart from the mechanisms mentioned above estuarine circulation may be modulated by local topographic features such as curvature (Becherer et al., 2015; Chant, 2002; Geyer, 1993) or channel convergence (longitudinally changing cross-estuary area, Burchard et al., 2014; Geyer & Ralston, 2015; Ianniello, 1979; Schulz et al., 2015).

The aim of this study is to understand the interplay of high variable coastal salinity, wind forcing, and river runoff, which can regularly drive a temporary reversed exchange flow and cause mixing in estuaries. Since this analyzes works best when the tidal mixing is low and the control mechanisms are therefore reduced to wind stress and buoyancy gradient forcing, this study uses realistic model results of a weakly tidal estuary as an example. The question is of how an estuary responds to changes in salinity and wind stress in terms of exchange flow, mixing, and stratification from a long- and short-term perspective and which parameters are suitable for description. This study is structured as follows: Diagnostic quantities and the study site are introduced together with the numerical model in section 2, followed by presentation of observational data in section 3.1 and numerical model results in section 3.2. Finally, results are discussed in section 4, and conclusions are drawn in section 5.

2. Methods

2.1. Diagnostic Quantities

The conventions used in this study are defined as follows: The Cartesian x-coordinate points into the estuary (longitudinal direction), the y-axis points cross-estuary (lateral direction), and the z-axis points upward, following the right-hand rule, with the corresponding velocity vector denoted as (u,v,w) and the abbreviated differential operator $\nabla = (\partial_x, \partial_y, \partial_z)$. With this, the seabed is located at $z=-H$ and the free surface at $z=\eta$ defining the total water depth as $D=\eta+H$. By using the buoyancy $b = -g\,\frac{\rho-\rho_0}{\rho_0}$ with the gravitational

acceleration $g = 9.81\,\mathrm{m\,s^{-2}}$ and the density ρ with its reference value of $\rho_0 = 1{,}025\,\mathrm{kg\,m^{-3}}$ as well as the longitudinal wind stress $\frac{\tau_x^s}{\rho_0} = u_*^s|u_*^s|$ and surface friction velocity u_*^s, the following essential non-dimensional parameters are defined as

- Simpson number $\mathrm{Si} = \partial_x b H^2/U_*^2$, describing the balance between stratification, caused by density gradient forcing, and destratification due to vertical mixing (Burchard et al., 2011; Stacey et al., 2010)
- Non-dimensional wind stress $\mathrm{Ts} = u_*^s|u_*^s|/U_*^2$, ratio of surface momentum flux to momentum flux at the seabed stating the relative strength of wind stress to bottom stress (Lange & Burchard, 2019)
- Local Wedderburn number $\mathrm{We} = u_*^s|u_*^s|/(\partial_x b H^2) = \mathrm{Ts}/\mathrm{Si}$, measure for the competition between gravitational forcing and wind forcing in driving estuarine circulation (Lange & Burchard, 2019; Purkiani et al., 2016)

where the reference bottom friction velocity scale

$$U_* = \left\langle \left(u_*^b\right)^2 \right\rangle^{1/2}, \tag{1}$$

has been used, with the bottom friction velocity u_*^b. For any quantity X, the time averaging operator $\langle\cdot\rangle$ and the volume-average $\widehat{\cdot}$ are defined as

$$\langle X\rangle(t_0) = \frac{1}{T}\int_{t_0-T/2}^{t_0+T/2} X(t)\mathrm{d}t \text{ and } \widehat{X} = \frac{1}{V}\int X(x,y,z)\mathrm{d}V, \tag{2}$$

with the averaging period T and the averaging volume V denoting the total estuarine volume in this study. Based on this, the temporal variance $\langle X'^2\rangle$ and spatial variance $\widehat{X^{*2}}$ are defined as

$$\langle X'^2\rangle = \langle (X-\langle X\rangle)^2\rangle \text{ and } \widehat{X^{*2}} = \widehat{\left(X-\widehat{X}\right)^2}, \tag{3}$$

respectively.

To quantify the importance of longitudinal wind stress and density gradient on the strength of the non-dimensional exchange flow through an estuarine cross-section, a dimensionless circulation parameter $\tilde{I}$ is used:

$$\tilde{I}(\tilde{u}) = -\frac{4}{\langle A\rangle}\int_0^L \langle D(y)\rangle \int_{-1}^0 \langle \tilde{u}(y,z)\rangle \left(\tilde{z}+\frac{1}{2}\right)\mathrm{d}\tilde{z}\mathrm{d}y, \tag{4}$$

with the non-dimensional velocity $\tilde{u} = u/U_*$, the cross-estuarine transect area $\langle A\rangle = \int_0^L \langle D(y)\rangle\,\mathrm{d}y$, the width of the transect L, and the non-dimensional water depth $\tilde{z} = z/H$. $\tilde{I}$ is defined in a way that a hypothetical exchange flow with $\tilde{u} = +u_c$ below mid-depth and $\tilde{u} = -u_c$ above mid-depth would result in $\tilde{I} = u_c$. Note that although (4) was originally introduced for the analysis of two-layer velocity profiles, the definition is robust for more complex situations with, for example, three layers.

With this, three situations can be distinguished: $\tilde{I} > 0$ describes classical (or positive) estuarine circulation, $\tilde{I} < 0$ is a reversed (or negative) circulation direction with inflow near the surface and outflow near the bottom, and the special case $\tilde{I} = 0$ describes situations where the drivers of the estuarine circulation cancel out each other. An analytical solution for the critical condition $\tilde{I} = 0$ is given by

$$\mathrm{Ts}_c = \mathrm{Si}\cdot\mathrm{We}_b + \alpha\cdot\tilde{U}_r \Leftrightarrow \mathrm{We}_c = \mathrm{We}_b + \frac{\alpha\cdot\tilde{U}_r}{\mathrm{Si}}, \tag{5}$$

where α is a constant and $\tilde{U}_r = u_r/U_*$ is a non-dimensional formulation of the residual flow velocity u_r. Equation 5 states that if the actual Wedderburn number is larger than a critical value ($\mathrm{We} > \mathrm{We}_c$), the circulation direction will be negative. Lange and Burchard (2019) showed that this critical Wedderburn number is composed of an estuary-specific basic Wedderburn number We_b, which is largely a constant value for a study site, and a dynamic term depending on the actual Simpson number and the non-dimensional residual flow velocity.

In order to investigate the fluxes corresponding to the estuarine exchange flow MacCready (2011) proposed a transformation from the Eulerian parameter space into an isohaline parameter space described in the framework of the TEF:

$$q(S) = -\frac{\partial Q(S)}{\partial S} \quad \text{and} \quad Q(S) = \left\langle \int_{A(S)} u \mathrm{d}A \right\rangle, \tag{6}$$

where q is the net volume transport per salinity class and $A(S)$ is the cross-sectional transect area with salinities larger than S. The corresponding inflow and outflow salinities are calculated as

$$s_{\mathrm{in}} = \frac{Q^s_{\mathrm{in}}}{Q_{\mathrm{in}}} \quad \text{and} \quad s_{\mathrm{out}} = \frac{Q^s_{\mathrm{out}}}{Q_{\mathrm{out}}}, \tag{7}$$

with the inflow and outflow salt flux Q^s_{in} and Q^s_{out} and volume transport Q_{in} and Q_{out}, respectively (Burchard et al., 2019; Geyer & MacCready, 2014; MacCready, 2011):

$$Q^s_{\mathrm{in|out}} = \int s q^{\mathrm{in|out}} \mathrm{d}s \quad \text{and} \quad Q_{\mathrm{in|out}} = \int q^{\mathrm{in|out}} \mathrm{d}s, \tag{8}$$

where the inflow contribution of a quantity X is calculated as $(X)^{\mathrm{in}} = \max(X,0)$ and the outflow contribution as $(X)^{\mathrm{out}} = \min(X,0)$. The analysis of discrete model data is described in Klingbeil et al. (2019) and Lorenz et al. (2019). Based on the TEF framework, MacCready et al. (2018) found by analysis of a salinity variance budget that the long-term averaged and volume-integrated salinity mixing M in an estuary can be approximated as

$$M = \left\langle \int_V \chi^s \mathrm{d}V \right\rangle \tag{9a}$$

$$\approx s_{\mathrm{in}}\, s_{\mathrm{out}} Q_r, \tag{9b}$$

with river discharge Q_r, the local salt mixing $\chi^s = 2\left[K_h(\partial_x s)^2 + K_h\left(\partial_y s\right)^2 + K_v(\partial_z s)^2\right]$, and the horizontal and vertical eddy diffusivity K_h and K_v, respectively. Here, mixing is used as a measure for the rate of destruction of salinity variance $\widehat{s^{*2}}$. Based on (9b), MacCready et al. (2018) and Burchard et al. (2019) showed that for classical estuarine circulation the ratio of actual mixing to the maximum possible mixing $M_C = M/M_{\max} = s_{\mathrm{in}}\, s_{\mathrm{out}} Q_r / s_{\mathrm{in}}\, s_{\mathrm{in}} Q_r = s_{\mathrm{out}}/s_{\mathrm{in}}$ estimates the mixing completeness of an estuary in terms of inflow and outflow salinities.

Finally, the potential energy anomaly ϕ (Burchard & Hofmeister, 2008; Simpson, 1981) is used as a measure for the strength of local stratification:

$$\phi = \frac{1}{D}\int_{-H}^{\eta} g z(\overline{\rho} - \rho) \mathrm{d}z, \tag{10}$$

with the depth-averaged density ρ. The potential energy anomaly is equal to the energy needed to instantaneously homogenize the entire water column, with larger values corresponding to larger stratification.

2.2. Study Site

The Warnow River Estuary is located at the German coast of the southwestern Baltic Sea (see Figure 1) in the city of Rostock. Its river discharge varies seasonally with typical values between 50 $\mathrm{m^3\,s^{-1}}$ in February and 5 $\mathrm{m^3\,s^{-1}}$ in August with an annual mean value of about $Q_r = 15\ \mathrm{m^3\,s^{-1}}$. The discharge into the estuary is highly variable in time, as it is controlled by a weir, which limits the spatial extent of the estuary to the south. In the north the estuary is bounded by two pier heads with a distance of 230 m, which also serve as endpoints of the transect later used for further analyses. In addition, the shoals are largely artificially fortified, since the Warnow estuary plays a large role in tourism and industry. Because of these barriers, the boundaries of the study site are well defined leading to a total estuary length of about 13 km and a mean water depth of 5.6 m. Deepest points in the estuary are located in the dredged shipping channel with a depth of about 15 m

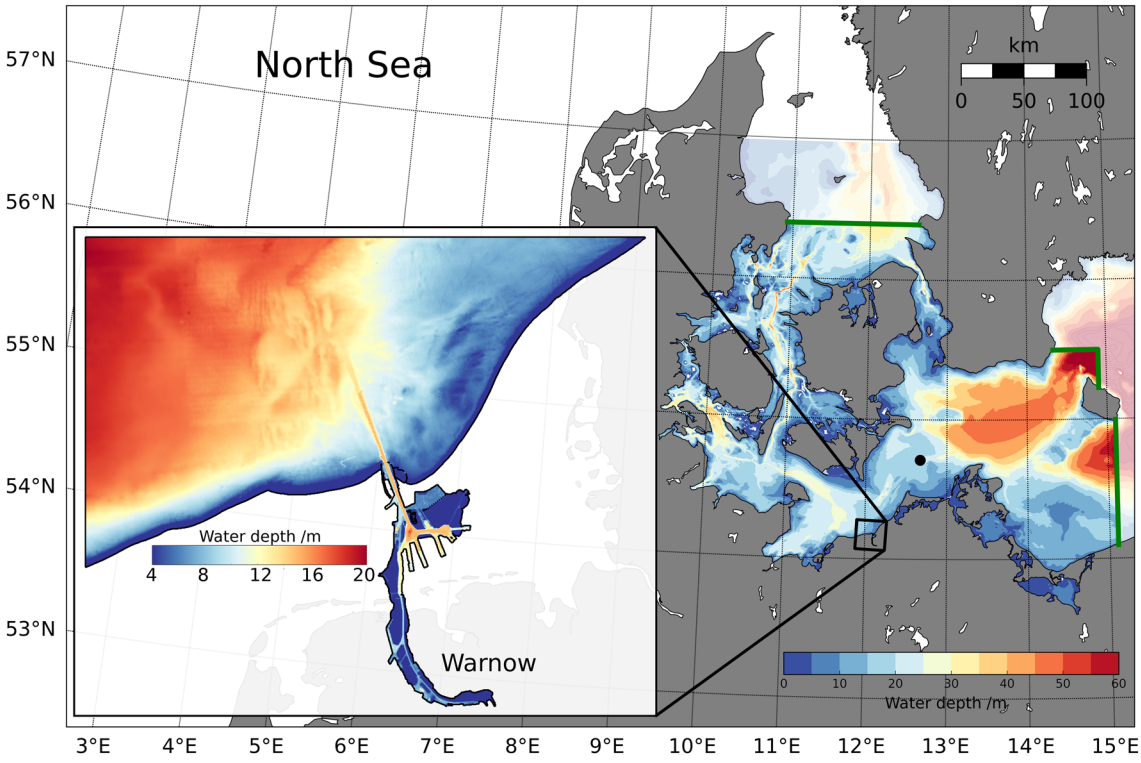

Figure 1. Water depth and expanse of the 20 m model of the Warnow estuary (left) and of the 200 m model of the western Baltic Sea (right). Open boundaries of the latter are highlighted in green, with the larger-scale model (600 m) in semi-transparent. The position of the measurement station "Darss Sill" is marked as a black dot.

reaching 5.5 km into the adjacent Bay of Mecklenburg (Figure 1). Due to this channel, the Warnow estuary is hydrologically connected with deeper parts of the ambient coastal water. The semi-diurnal M_2-tide has an amplitude of about 8 cm which is why the Warnow estuary can be considered as a micro-tidal estuary, synonymously referred to as weakly tidal in the following. Because the estuary is located midlatitude and thus in the region of the prevailing westerlies, the largest wind velocities are observed coming from west to north-west.

2.3. The Numerical Model

The numerical simulations in this study were carried out with the General Estuarine Transport Model (GETM) (Burchard & Bolding, 2002; Hofmeister et al., 2010; Klingbeil & Burchard, 2013) using the General Ocean Turbulence Model (GOTM) (Burchard et al., 1999; Umlauf & Burchard, 2005) as turbulence closure model (second-order, k–ε). GETM is a three-dimensional numerical model that solves the Reynolds-averaged Navier-Stokes equations under Boussinesq approximation by using the finite-volume approach (see review in Klingbeil et al., 2018). It was developed for studying coastal ocean processes and has been successfully applied in numerous studies (e.g., Gräwe et al., 2015, 2016; Holtermann et al., 2014). GETM is used for modeling exchange processes (Purkiani et al., 2016), dynamics of sediments (Sassi et al., 2015), particle tracking (Gräwe & Wolff, 2010), and bio-geo-chemistry (Schiele et al., 2015).

In this study the simulations were performed in two steps: A large-scale model, covering the region of the western Baltic Sea, was applied in order to calculate boundary conditions for the subsequent simulations of the smaller-scale model of the Warnow estuary and its ambient coast. The model for the western Baltic Sea makes use of a numerical grid in 200 m spatial resolution and 40 vertical layers with their layer height adapting to the vertical density gradient (Gräwe et al., 2015; Hofmeister et al., 2010). Time series of water temperature, salinity, horizontal velocities, and water level at the open boundaries of the 200 m model (highlighted in green in Figure 1) are obtained from output of a larger-scale model of the western Baltic Sea with a resolution of 600 m (see Gräwe et al., 2015, for details). Since the 200 m model has two open boundaries and

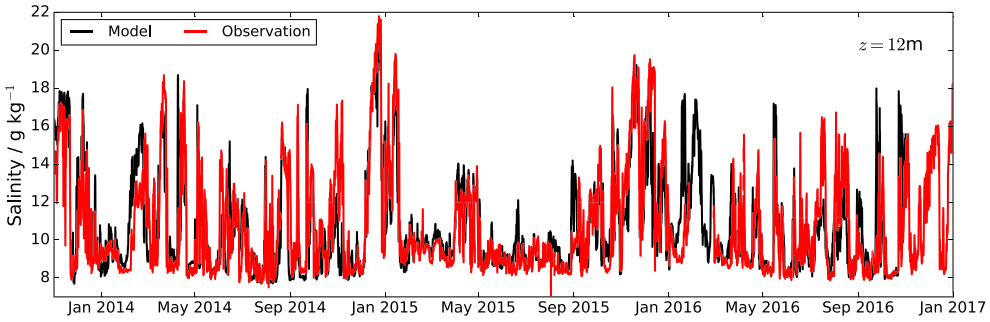

Figure 2. Mid-depth salinity measured at station Darss Sill (red) compared to calculated model results (black) for the western Baltic Sea in 12 m depth.

its hydraulic resistance is different than in the 600 m model, the barotropic pressure gradient has been calibrated to compensate for the deviating salinity transports (see, e.g., Burchard et al., 2009). Meteorological forcing is calculated from output of the German Weather Service Local Model (DWD-LM) with 3 hr temporal and 7 km spatial resolution. The resulting model output of the 200 m model is subsequently used to force the small-scale model of the Warnow estuary at its open boundaries (shown in black in Figure 1).

The model domain of the Warnow estuary and its adjacent coast are discretized on a structured numerical grid with a horizontal resolution of 20 m using Cartesian coordinates and 25 equidistant bottom-following σ-coordinates. For the meteorological forcing the same underlying data set as in the large-scale 200 m model is used. The daily-averaged values for the discharge of the Warnow river are provided by the Office for Agriculture and Environment Mittleres Mecklenburg. Both models have a spin-up time of 1 year, starting from initial conditions of temperature and salinity, spatially interpolated from their larger-scale outer model, respectively. In the following, this study focuses exemplarily on the results for the year 2014, as most of the validation data for the estuary are available during this period.

2.4. Model Validation

Before the numerical results, calculated by the 200 and 20 m models, are used for further analysis, their quality is estimated by comparison with observational data. The focus here is especially on the reproduction of the observed salinity, as it largely determines the density and thus the buoyancy gradient as an important driver of estuarine circulation. Note that the temperature plays only a minor role in changing the density in the western Baltic Sea. A nearby measurement station is the autonomously operating measurement tower *Darss Sill* (marked in Figure 1) which is part of the MARNET network for marine ecosystem monitoring in the North Sea and the Baltic Sea. Results show that the large-scale 200 m model of the western Baltic Sea reproduced most of the inflow events of saline water in good agreement with observations (exemplarily shown for mid-depth [12 m] in Figure 2). Note that the specific position of the station at Darss Sill aims to identify inflow of high saline (and usually oxygen-rich) water originating from the North Sea, into deeper layers of the central Baltic Sea (Burchard et al., 2018; Gräwe et al., 2015).

Figure 3 compares output from the 20 m model of the Warnow estuary in black to observations in red in terms of water level (a), bottom temperature (b), and bottom salinity (c) for the year 2014. The underlying observational data for temperature and water level are provided by the Office for Agriculture and Environment Mittleres Mecklenburg, and the salinity is calculated from conductivity measurements of a CTD-probe (Conductivity-Temperature-Depth).

The measured water level includes small tidal variations which is successfully reproduced by the numerical model in terms of timing as well as magnitude. Larger variations of the sea level in the estuary are mainly driven by changes of the water level in the western Baltic Sea caused, for example, by storm events and the resulting compensation movements. The water level is reproduced by the model with a coefficient of determination of $r^2 = 0.84$ and a root mean square error (rmse) of 8.3 cm. The observed and modeled temperature follow a yearly cycle with a highest value of $\theta = 22.3$°C in August and a lowest value of $\theta = 1.2$°C in February. Observations and numerical simulations agree well with an r^2 value of 0.99 but with the

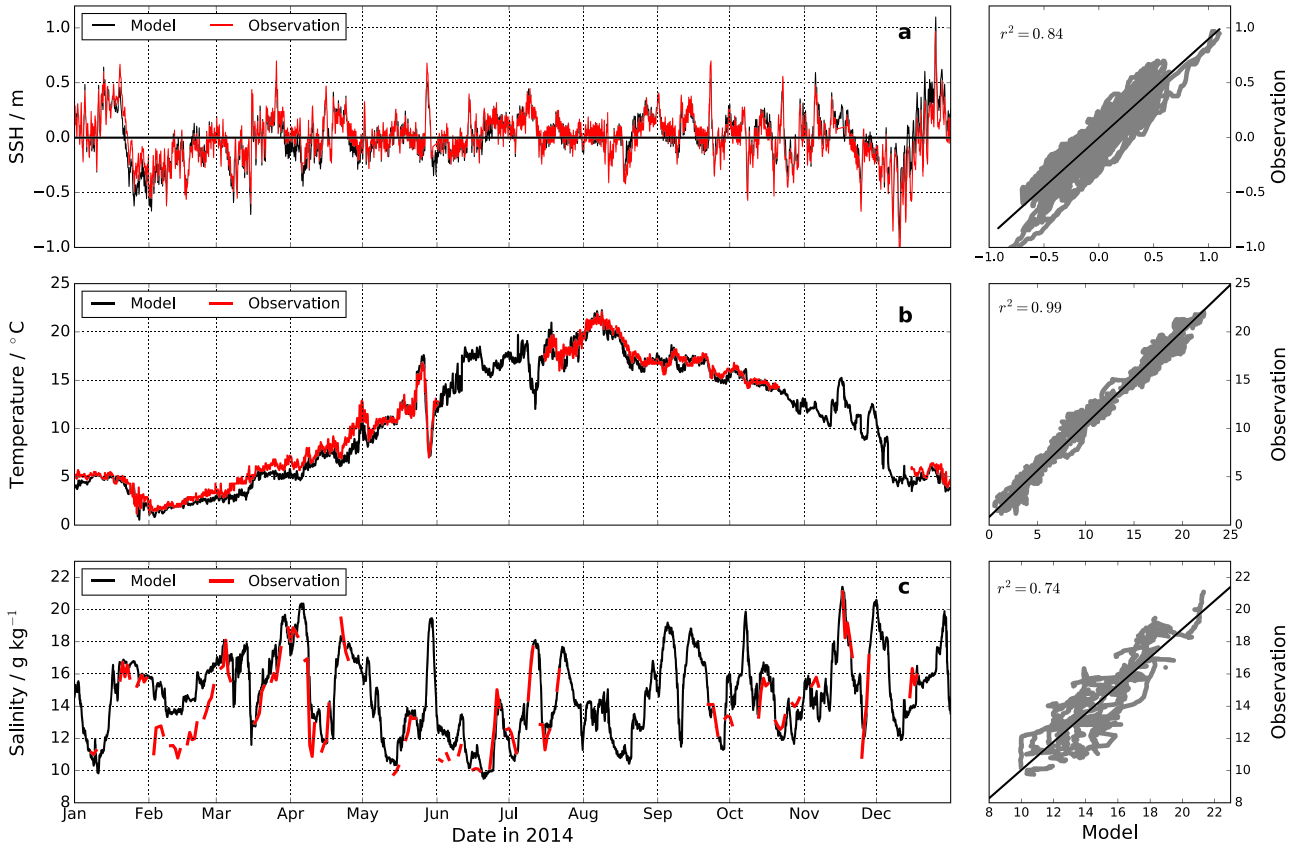

Figure 3. Observation of sea level (a), bottom water temperature (b), and bottom salinity (c) in the Warnow estuary in red compared to model results in black for the year 2014.

model slightly underestimating the bottom temperature between March and May resulting in an rmse value of 0.8°C. The exceptionally strong upwelling event at the end of May, where the temperature dropped by about 10°C within 2 days, is captured by the model in good agreement to measured data in time and magnitude. The bottom salinity (Figure 3c) shows large variations in a range between 9.5 and 21.4 g kg^{-1}. Daily values of measured salinity indicate that the modeled salinity is overestimated in February, which is due to overestimated salinities in the 200 m model of the western Baltic Sea (see February 2014 in Figure 2) passing the error via the open boundaries into the small-scale model. However, in general, the inflow events into the estuary (increased salinity peaks) are well reproduced by the model with $r^2 = 0.74$.

2.5. Mixing in the Estuary

While the inflow volume transport only takes place in a small salinity range corresponding to the bottom salinity outside the estuary, the outflow may extend over several salinity classes due to salinity mixing processes in the estuary (Figure 9d). In order to estimate the degree of mixing for the Warnow estuary, the inflow and outflow salinities s_{in} and s_{out} for the transect at the mouth are consistently calculated in the TEF framework (7) from the time series shown in Figure 9d. Each data point in the s_{in}–s_{out} parameter space (Figure 4) represents a certain point in time in 2014 while the color code gives the respective strength of the exchange flow I (see Figure 9c). The solid line represents a unity line, indicating equal values of inflow and outflow salinity, dividing the parameter space in two sections with (I) $s_{out}/s_{in}<1$ and (II) $s_{out}/s_{in}>1$.

Data points in Section II represent situations with water leaving the estuary having a higher salinity than water entering the estuary, which is the case when the circulation direction is reversed ($I<0$ in blue) and high saline bottom water is transported seaward. In contrast to this, classical estuarine circulation ($I>0$), with low saline surface water leaving the estuary, is represented by data shown in Section I in red. A linear regression through data points within a positive circulation, indicated as a dashed line, gives a

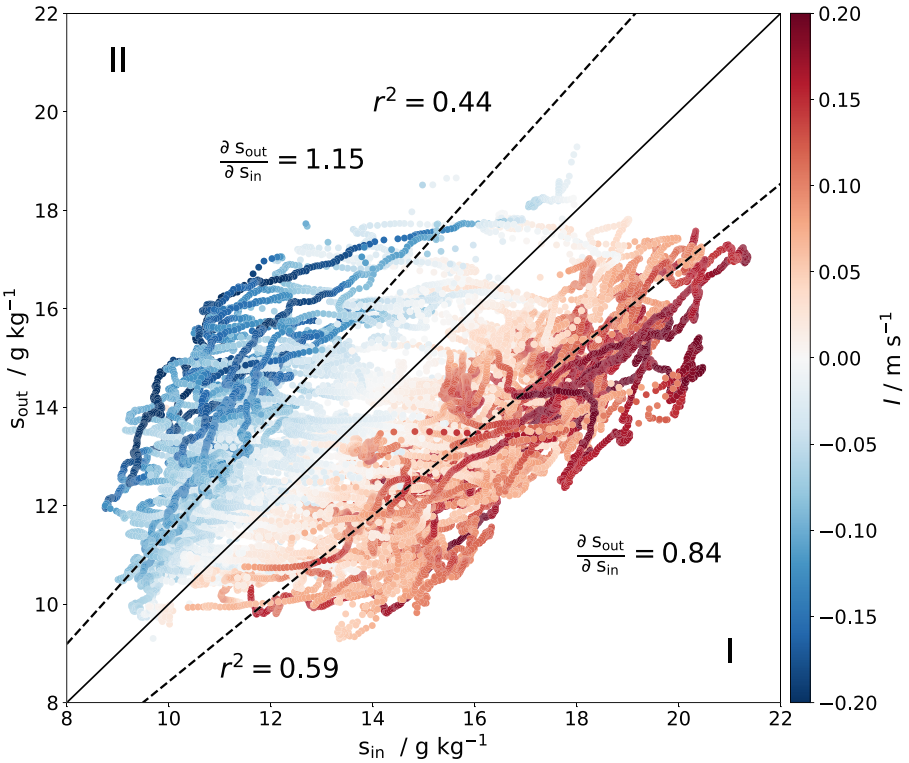

Figure 4. Relationship between outflow salinity s_{out} and inflow salinity s_{in} for classical (red) and reversed (blue) estuarine circulation, with the color code giving the corresponding strength of the exchange flow I. The dashed lines are linear regressions through data points within a common circulation direction, and the solid line represents the unity condition s_{out}=s_{in} for comparison.

relationship how the outflow salinity changes with respect to s_{in}. The slope of the regression has a value of $\frac{\partial s_{out}}{\partial s_{in}} = M_C = 0.84$ stating that the outflow salinity is about 84% of the inflow salinity.

While this regression only represents a long-term average, the instantaneous estuarine-wide mean salinity $\hat{s}$ is still a function of time (Figure 5a). Its value is generally increasing in the presence of a positive circulation, since saline coastal bottom water is transported into the estuary, and decreases if the exchange flow reverses its direction ($I < 0$). This dependence of the estuarine-wide salinity on the strength of the exchange flow highlights the applicability of I for system-wide descriptions even though it is calculated only for a transect at the mouth of the estuary.

Besides the spatially averaged salinity $\hat{s}$, its volume-integrated deviation $S_V^{*2} = \int s^{*2} \mathrm{d}V$ and the mixing M give insights into the estuarine dynamics (Figure 5b). Here, the latter is calculated as the sum of numerical and physical mixing obtained from output of the exact mixing analyses in the numerical model (Klingbeil et al., 2014). Results show that the analytical estimation of the salinity mixing (blue) defined in (9b) is in good agreement with the exact mixing (red) although there are some deviations. In general, the mixing increases when the salinity variance increases, while the latter results from inflow of high saline water into the estuary (Figures 3 and 5a).

The ratio of total salinity variance S_V^{*2} to total mixing M has the dimension of a timescale T_{mix}:

$$T_{mix} = \frac{S_V^{*2}}{M}, \tag{11}$$

which can be interpreted as the time needed to homogenize the estuarine-wide salinity distribution (Figure 5b) by using the actual mixing. Results show that the typical mixing timescale for the Warnow estuary is in the order of $T_{mix} \approx 1$ day (red line in Figure 5c), which is exceeded at certain events during

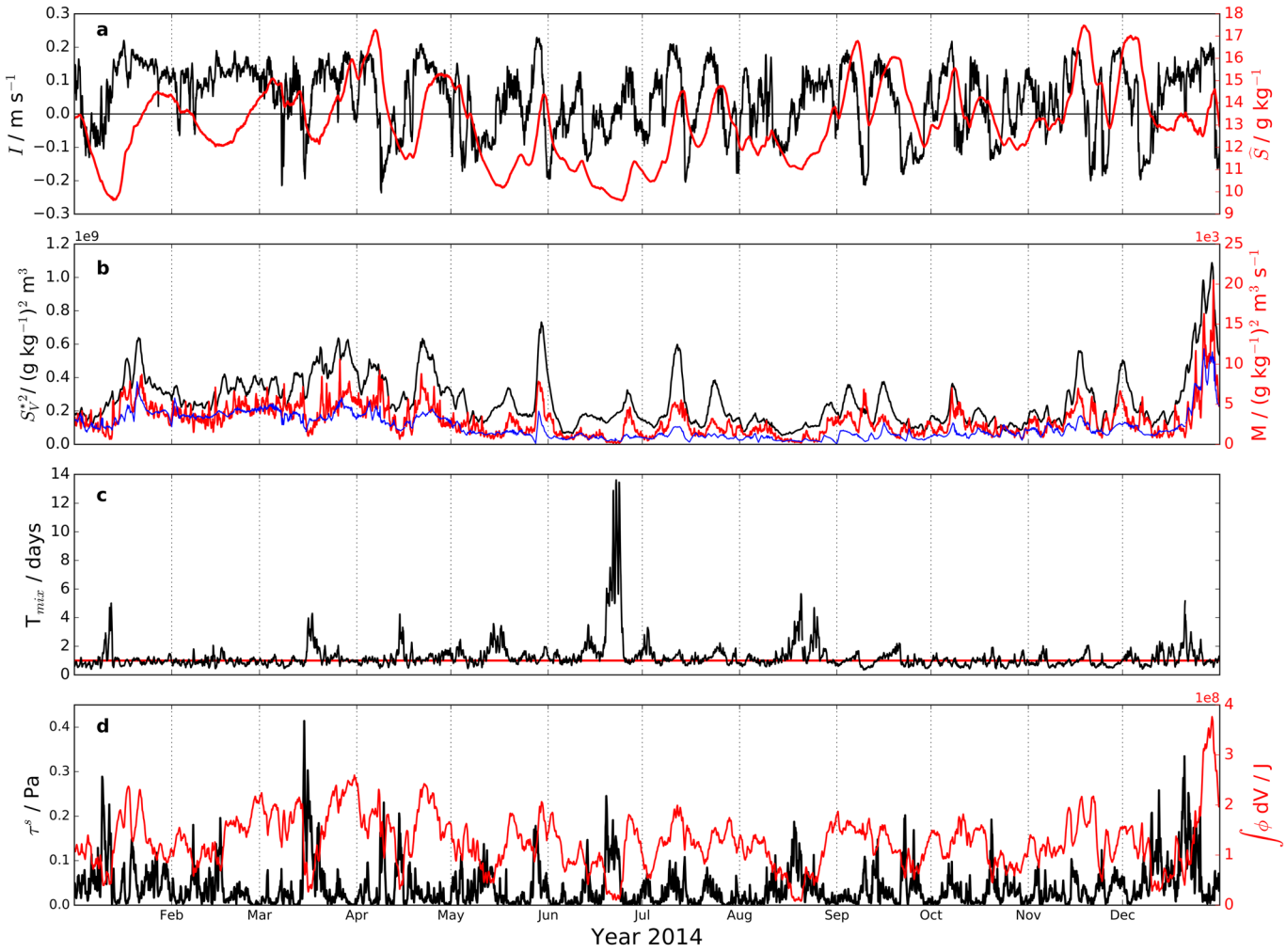

Figure 5. Mixing analysis for the Warnow estuary. (a) Strength of Total Exchange Flow I at the mouth in black and estuarine averaged salinity $\hat{s}$ in red. (b) Volume-integrated salinity variance S_V^{*2} (black) compared to total mixing in the estuary calculated by the numerical model (red) and by the analytical approximation (9b, blue). (c) Mixing timescale S_V^{*2}/M in black and the 1 day line for reference (red). (d) Absolute surface stress τ^s (black) and the volume-integrated potential energy anomaly in red.

the year to 3–4 days and in June even to 1–2 weeks, resulting from small values of M (Figure 5b). The reduced mixing can be explained by analyzing the density stratification in terms of the spatially integrated potential density anomaly φ, as defined in (10), representing the total energy needed to homogenize the individual water columns in the estuary vertically (Figure 5d). Smaller values of φ indicate reduced stratification, suggesting that the water column is well mixed locally. As a result, the values of M decrease, as already mixed water cannot be further mixed. The vertically low stratification at certain events coincides with larger values of wind stress (shown in red), indicating a decrease of φ due to wind-induced mixing. Note that the vertically mixed water may still have a horizontal salinity gradient (see also Figure 8a) resulting in a still existing total salinity variance.

3. Results

3.1. Observations

In order to get a broader overview about the dynamics in the near-estuary coastal area, the sea surface temperature (SST) in the western Baltic Sea is calculated from radiances measured by the Earth observation satellite Landsat 8 for a situation in March and July in 2014 (Figures 6a and 6b). For that its spectral band 10 (wavelength: 10.3–11.3 μm) with a spatial resolution of 100 m and a swath width of 185 km has been

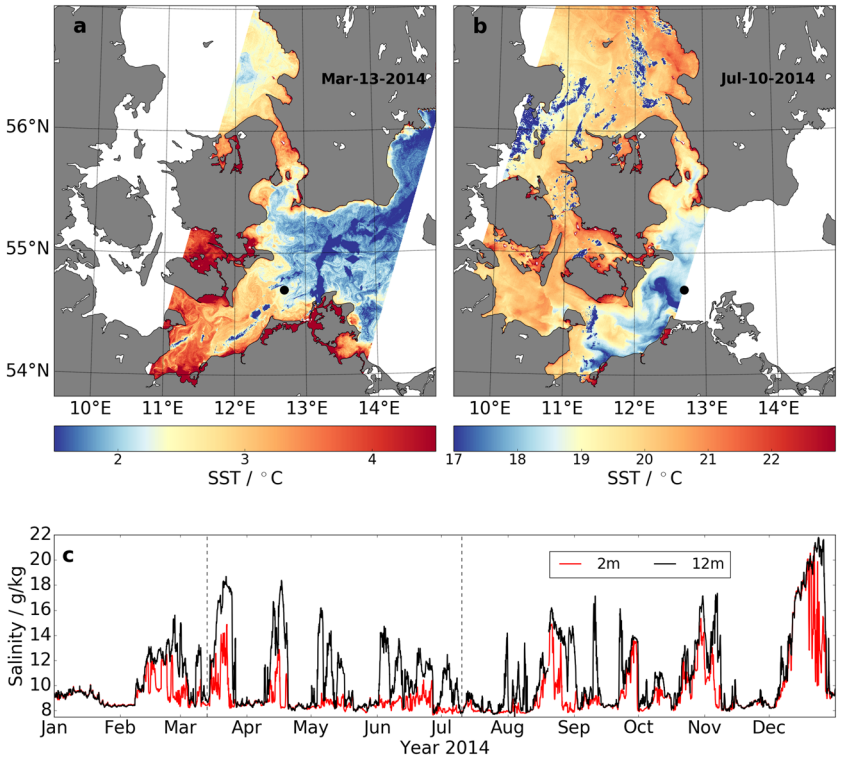

Figure 6. Sea surface temperature (SST) in the Bay of Mecklenburg and parts of the western Baltic Sea calculated from satellite radiances for a situation in (a) March and (b) July 2014. (c) Time series of observed salinity in 2 m depth in red and mid-depth in black (12 m). The black dot denotes the corresponding position of the measurement tower Darss Sill. Irregular dark blue patterns are caused by clouds.

used. Atmospheric correction is applied by using upwelling and downwelling radiances as well as the transparency of the atmosphere calculated using a model of a standard atmosphere (for details, see, e.g., Barsi et al., 2003). Both measurements show a lateral gradient in temperature where warmer water is found in the west and colder water in the east with a difference of about 2°C. The origin of these two different water bodies is identified by considering salinities observed in 2014 by the stationary measurement tower located at Darss Sill (Figure 6c). The near-surface salinity (2 m depth) in red varies between 8 and 15 g kg^{-1} while the mid-depth salinity (12 m depth) varies between 8 and 19 g kg^{-1}. While in July the colder water has a low surface salinity with values of $s \approx 8$ g kg^{-1}, the situation in March, with warmer water approaching the measurement tower, is captured just a day before the surface salinity increased from 8.5 to 12 g kg^{-1}. This indicates that the warmer water body has a higher salinity than the colder one, suggesting its origin in water from the North Sea with different properties than the brackish water of the Baltic Sea in the east. Since the shipping channel of the Warnow estuary has a depth of about 15 m, increases of salinity in mid-depth potentially increase the salinity in the estuary as well. With this, the Warnow estuary is located in a zone strongly influenced by two different water masses resulting in an exposure to ambient water with high salinity (Figure 6a) as well as with low salinity (Figure 6b) leading to the high variability shown in Figure 3. The time series in Figure 6c indicates that changes in salinity (even a doubling) can occur on short time scales of within 2–3 days.

3.2. Model Results

In addition to the observed temperature gradient, numerical simulations of the western Baltic Sea averaged over the year 2014 show a lateral salinity gradient in the surface water with salinities larger than 20 g kg^{-1} in the north-west and about 8 g kg^{-1} in the east (Figure 7a). The corresponding bottom salinities are larger in the deeper parts and approximately follow bathymetric features. Results show that the near-bottom currents are generally directed into the Baltic Sea, indicating an inflow of higher saline water with increased current speeds in the channels (Figure 7d), while the velocities at the surface indicate an outflow of near-surface

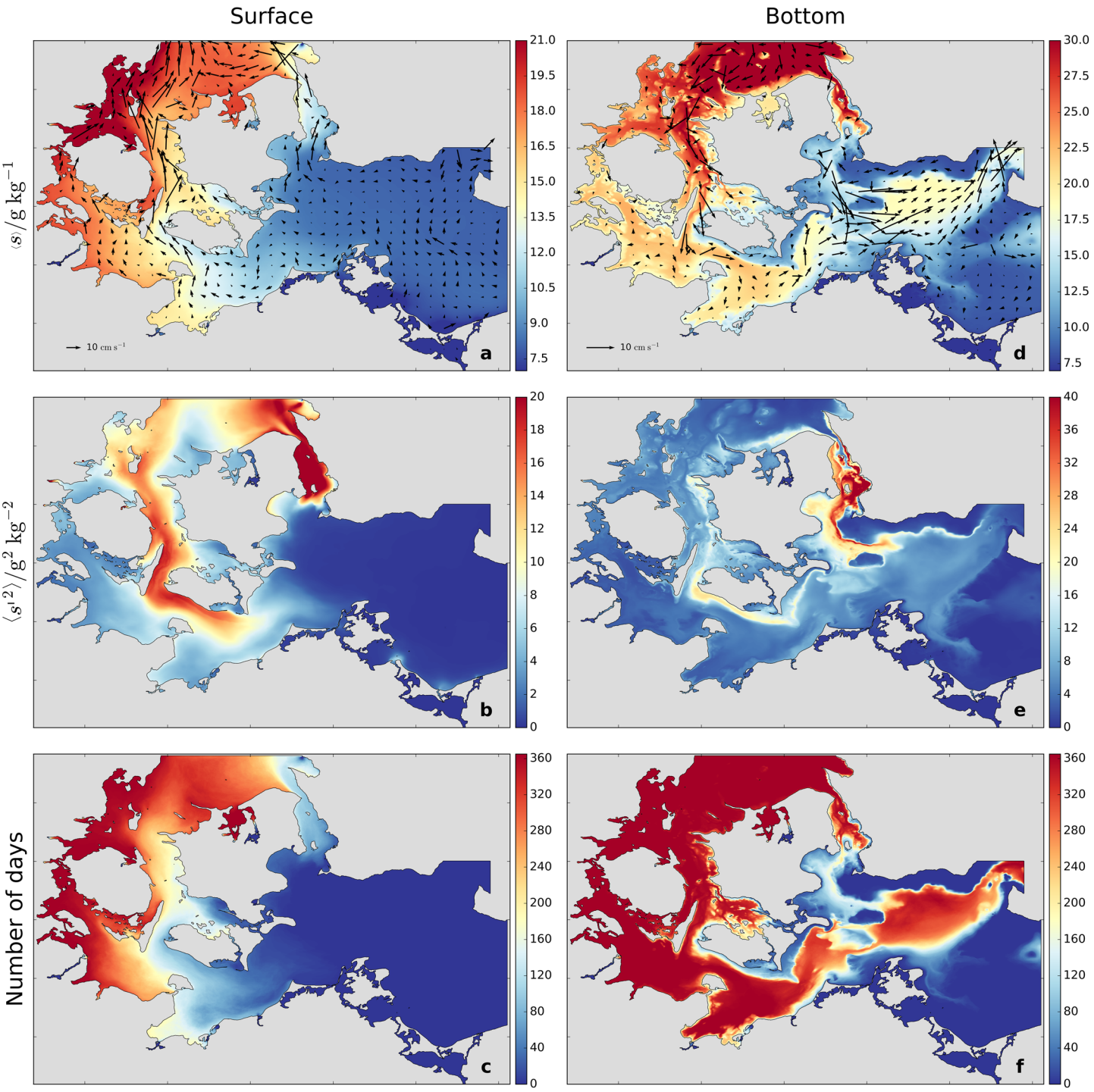

Figure 7. Annually averaged salinity (a,d) and its temporal variance (b,e) at the surface and at the bottom, respectively. The corresponding number of days with salinities larger than 15 g kg^{-1} is shown in (c) and (f). Arrows represent the mean current velocity. The underlying data are obtained from a numerical model for the year 2014.

water. This bidirectional exchange flow indicates that the western Baltic Sea shows the flow characteristics of a classical estuary with saline water being transported into the system, which is then mixed and transported outward (Burchard et al., 2018; Knudsen, 1900). Note that the long-term freshwater discharge into the Baltic Sea is estimated as approximately 15,200 m^3 s^{-1} (Matthäus & Schinke, 1999). The annual

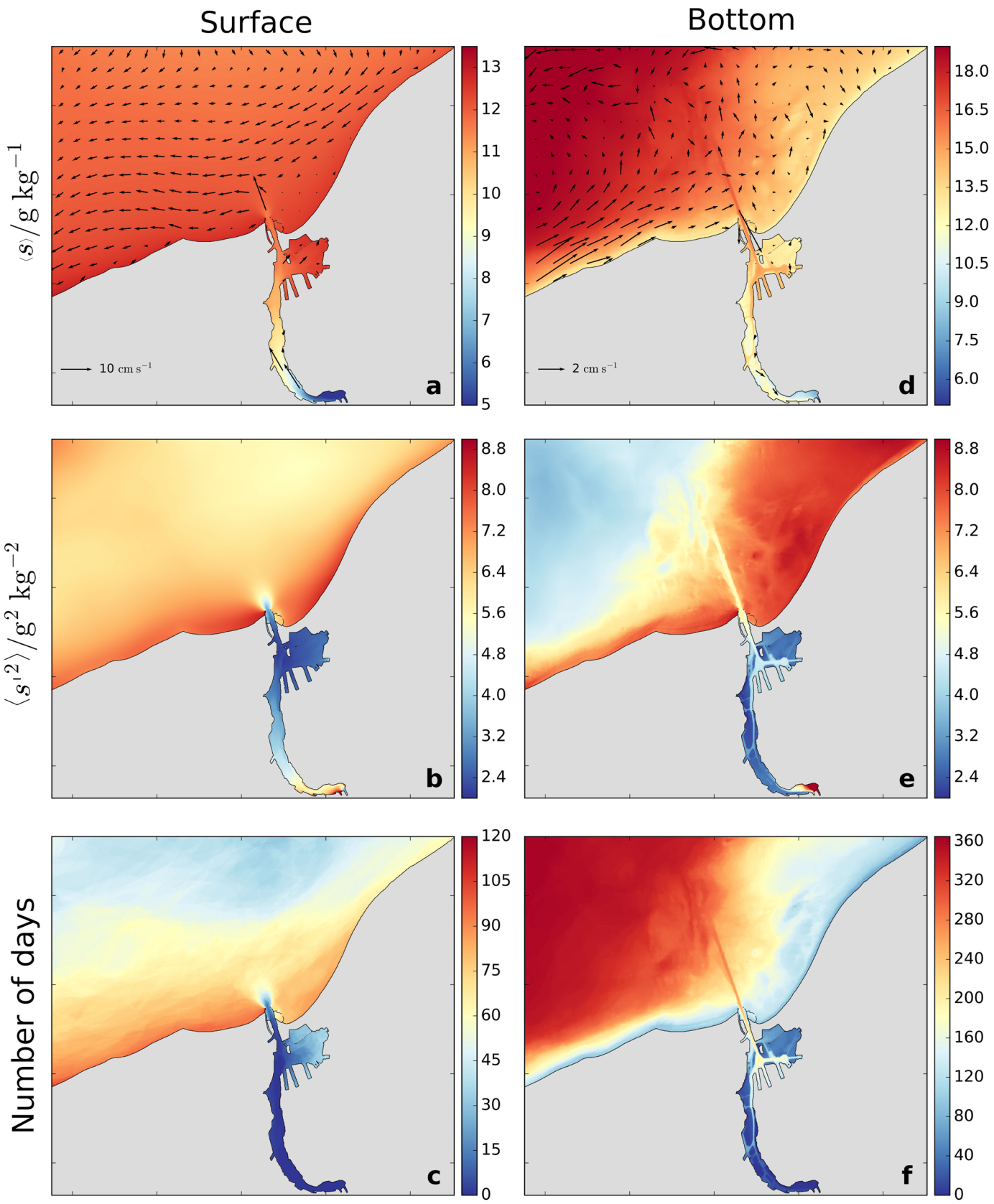

Figure 8. Same as in Figure 7 but showing model results obtained for the Warnow estuary. Note the different scales in the panels.

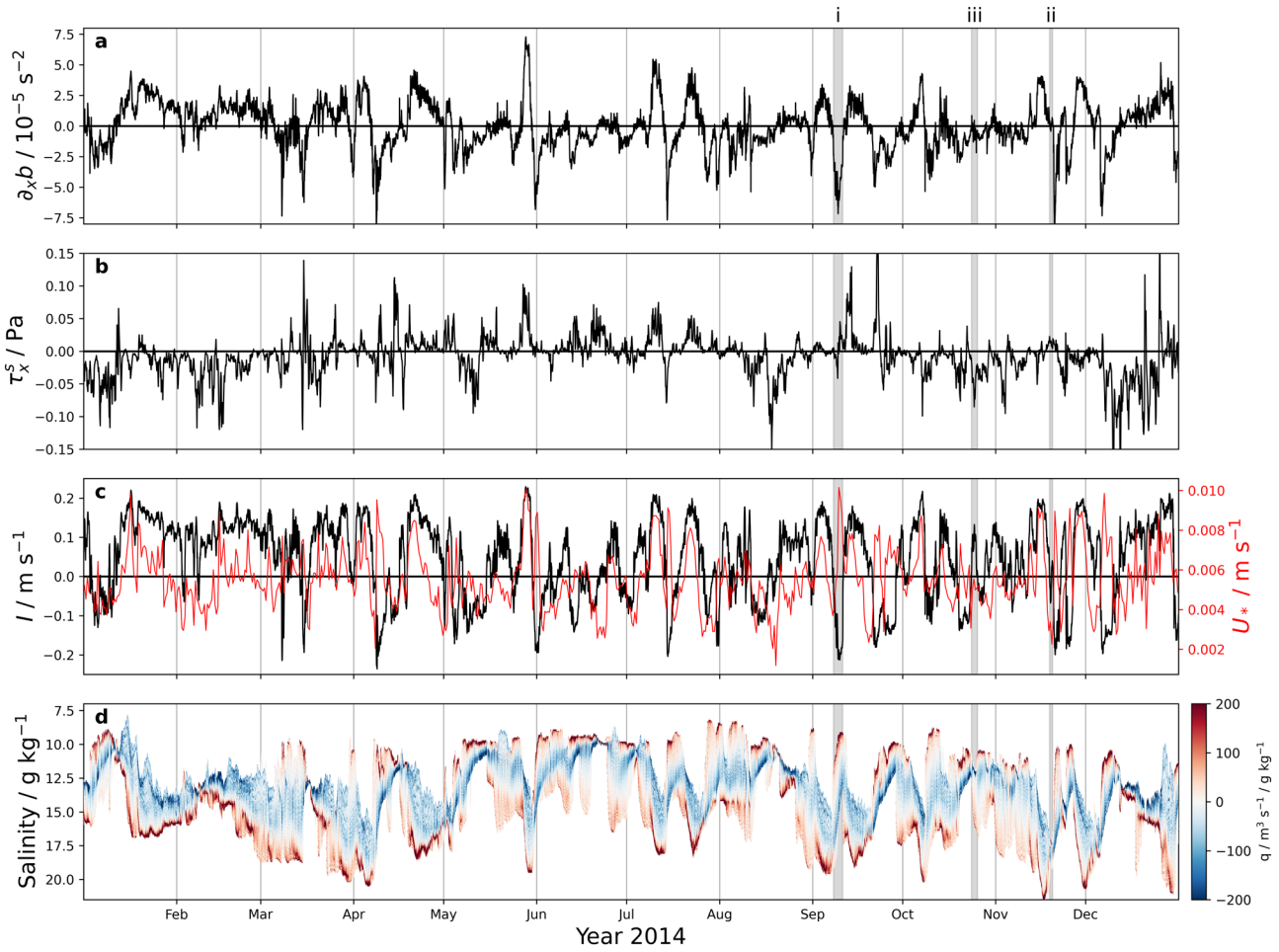

Figure 9. Transect-averaged longitudinal buoyancy gradient (a), wind stress (b), and strength of estuarine circulation (black) as well as bottom friction velocity scale (red) (c) at the mouth of the Warnow estuary calculated with a numerical model. The corresponding volume transport per salinity class is shown in (d). Shaded areas are examples of different realizations of inverse estuarine circulation.

salinity variance $\langle s'^2 \rangle$, calculated using deviations of daily-averaged values from its annual mean, is small (<2 $(g/kg)^2$) at the surface in the eastern part of the western Baltic Sea, indicating only minor temporal changes in salinity (Figure 7b), while its value increases to 6–8 $(g/kg)^2$ in the western parts, which include the coastal area in front of the Warnow estuary. This highlights the variability of salinity due to the changing water bodies observed in Figure 6. The latter is underlined when counting the days with salinities larger than 15 g kg^{-1} (Figure 7c). Simulations show that at the surface in the west this threshold value is exceeded on every day of the year 2014 while it is never reached in the eastern part. However, in the central area, including the coastal water in front of the Warnow estuary, increased salinities are found on about 120 days. Note that this (arbitrary) threshold of $s_{th} = 15$ g kg^{-1} is chosen as an intermediate value between typical maximum (20 g kg^{-1}) and minimum (10 g kg^{-1}) bottom salinities observed in the Warnow estuary (Figure 3c). Bottom salinities are almost always larger than s_{th} in the deeper channels and basins (Figure 7f).

When considering the higher resolved model results for the Warnow estuary, they confirm mean salinities of about 12 g kg^{-1} at the surface of the coastal water, as already found in the large-scale model, decreasing in the estuary when moving landward (Figure 8a). The salinity variance at the bottom indicates that the shallower coastal areas are exposed to larger variations in contrast to the deeper parts (Figure 8e). Besides the large-scale dynamics of high saline and brackish water in the western Baltic Sea, results show that the near-coastal water is additionally influenced by the effect of coastal upwelling, as indicated by increased values of days exceeding the threshold of 15 g kg^{-1} (Figure 8e). The bottom salinity highlights the role of

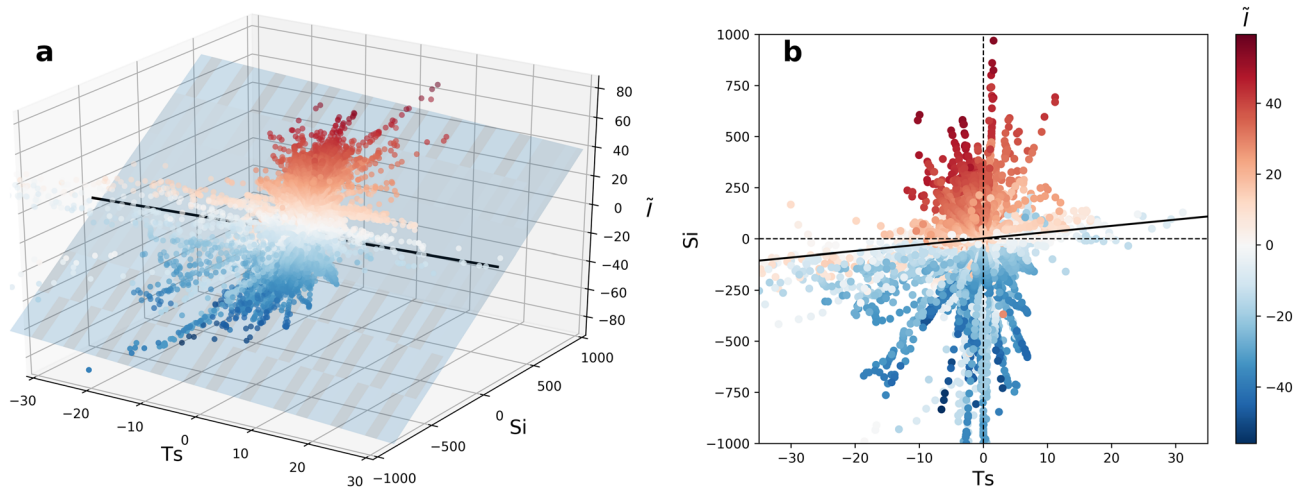

Figure 10. Strength of estuarine circulation $\tilde{I}$ dependent on varying Simpson number Si and non-dimensional wind stress Ts. The straight line indicates the critical condition $\tilde{I} = 0$ for the transition of classical circulation (red) to an inverted circulation (blue), obtained from a 3-D planar regression (a).

the shipping channel in connecting the estuary with the deeper and more saline offshore water (Figures 8d and 8f). Current velocities in this channel show a near-bottom up-estuary transport and a near-surface seaward transport verifying the existence of estuarine circulation in the Warnow estuary.

The volume transports per salinity class q, calculated according to the TEF framework (6), into and out of the estuary, associated with the exchange flow, show, similar to the dynamics in the western Baltic Sea, a high temporal variability (Figure 9d). The time series is calculated for a transect at the mouth of the estuary, with positive values in red meaning inflow (up-estuary) while outflow (negative) is shown in blue. Note that the salinity axis is inverted since in a stably stratified water column larger salinities are found near the bottom and lower salinities can be interpreted as being located near the surface. With this, classical estuarine circulation is described by inflow in high salinity classes and outflow in low salinity classes and reversed circulation correspondingly vice versa. The transition from positive to negative circulation is often connected with a shift in the salinity regime where the lowest occurring salinities decrease rapidly (see, e.g., Figure 9d at the end of May with a decrease in salinity from about 15 to 9 g kg^{-1}). This low saline water must originate from the outer ambient coastal area, since the volume transport in the low salinity classes points into the estuary (shown in red), underlining the findings of section 3.1 of an alternating salinity varying between relatively large values and more brackish ones in the western Baltic Sea. Since the outer changes in salinity may occur on short time scales (Figure 6c) compared to the estuarine adaption time to the new salinity, the density gradient potentially reverses its direction. Due to this, the resulting longitudinal buoyancy gradient $\partial_x b$ at the mouth (transect-averaged) varies in a range between -8 and $+8 \times 10^{-5}$ s^{-2} (Figure 9a). The corresponding strength of the estuarine circulation I generally follows the trend of the buoyancy gradient (Figure 9c) with a negative gradient resulting in an inverted circulation direction. However, when analyzing the frequency of inversion of the buoyancy gradient ($\partial_x b < 0$), it turns out that 49% of this occurred in 2014, while only 33% of the data show inversion for the estuarine circulation (I<0). This imbalance indicates that wind straining must be involved in additionally driving the exchange flow and opposing the gravitational forcing. Note that the adjustment time of I at the mouth to changes in buoyancy gradient and wind stress is in the order of up to 1 hr, so the inertia of the estuary plays only a minor role. By scaling $\partial_x b$, τ_x^s, and I with the bottom friction velocity scale U_*, according to the definitions presented in section 2.1, the sensitivity of the estuary with respect to wind straining can be estimated in terms of the basic Wedderburn number We$_b$. Lange and Burchard (2019) showed that the estuarine circulation $\tilde{I}$ is fully described in a parameter space spanned by the Simpson number Si and the non-dimensional wind stress Ts allowing the estimation of We$_b$ from the $\tilde{I} = 0$ condition. Contrary to their study, the Warnow estuary is a micro-tidal estuary with typical values of U_* found to be smaller than 1 cm s^{-1} (Figure 9c) and thus an order of magnitude smaller than friction velocities found in tidally energetic estuaries, resulting in much larger values of the Si, Ts, and $\tilde{I}$. However, results show that the non-dimensional exchange flow $\tilde{I}$, presented in a Ts-Si parameter space,

can still be distinguished between positive and negative circulation, shown in red and blue in Figure 10a, as suggested by Lange and Burchard (2019). The critical condition for cancellation of estuarine circulation by opposing wind stress and gravitational forcing $\tilde{I} = 0$ separates both states, indicated by a bold line. Its slope is obtained from a least squares surface regression (Figure 10a) according to $\tilde{I} = a \cdot \mathrm{Ts} + b \cdot \mathrm{Si} + c$, with (a, b, c) being fitting parameters, resulting in a basic Wedderburn number of $\mathrm{We}_b = 0.33$ for the Warnow estuary.

4. Discussion

In this study the Warnow estuary in the southwestern Baltic Sea is used exemplarily as a prototype for a weakly tidal estuary in a highly variable environment. Because tidal forcing plays only a minor role in driving estuarine circulation, the governing mechanisms are reduced to wind straining and buoyancy gradient forcing including the resulting effects of stratification and mixing. Results show that the formation of the buoyancy gradient in the estuary is driven by various processes: Large-area temperature observations in the western Baltic Sea, obtained from satellite data, local offshore time series of salinity measurements, and high-resolution model results suggest that the study site is exposed to strong changes in the outer water body, alternating between relatively high saline water and low saline brackish water originating from the North Sea and the Baltic Sea, respectively. In times of water with high salinity in front of the estuary, the results show that the buoyancy gradient is generally positive resulting in a classical circulation transporting the saline bottom up-estuary and therefore increasing the salinity in the estuary (see also Figure 5a). When the saline coastal water is replaced by the brackish water of the Baltic Sea, the density gradient at the mouth of the estuary is found to reverse its direction, since the salinity of the estuarine water is still increased by the former influx of saline coastal water. This suggests that in the Warnow estuary the salinity gradient can be temporally reversed similar to inverse estuaries found in arid regions (Johns et al., 2003; Nunes & Lennon, 1986). Contrary to the latter, the cause here is not strong evaporation but the storage of salt in the estuary in combination with the water exchange time of the estuary (flushing time ≈30 days, not shown) being larger than the time scale of changes in the ambient water, which can be in the order of 1–2 days (Figure 6c).

When further analyzing the density gradient and wind forcing in terms of Simpson number Si and non-dimensional wind stress Ts at the mouth of the river, it turns out that due to the missing tides the bottom friction velocity scale is much smaller ($\sim 10^{-3}\,\mathrm{m\,s^{-1}}$) than in tidally energetic estuaries ($\sim 10^{-2}\,\mathrm{m\,s^{-1}}$), leading to unusual large values of Si, Ts, and $\tilde{I}$. Note that the Simpson number was originally introduced for studying tidal mixing in estuaries (Simpson et al., 1990). Nevertheless, the method of calculating the basic Wedderburn number in the Si-Ts parameter space turns out to still be valid. When using a least squares surface regression method, the basic Wedderburn number results in $\mathrm{We}_b \approx 0.33$ for the Warnow estuary (Figure 10). This is only half of the value found by Lange and Burchard (2019) for a tidal inlet in the Wadden Sea ($\mathrm{We}_b \approx 0.6$) and smaller than the dynamic 1-D model result ($\mathrm{We}_b \approx 0.45$) but larger than the stationary analytical and dynamic non-tidal solution ($\mathrm{We}_b \approx 0.15$). A possible reason for this is that even in the absence of tidal forcing, wind straining still has to counter effects induced by lateral processes in addition to the gravitational circulation. The smaller basic Wedderburn number indicates that the exchange flow in the weakly tidal estuary is more sensitive with respect to wind stress than the estuarine circulation in the tidal energetic inlet in the Wadden Sea. This sensitivity is expressed in the fact that the intensity of the exchange flow in the Warnow estuary varies more with the wind for a constant buoyancy gradient than it would for larger Wedderburn numbers found in tidally driven estuaries.

With this, the results show that an inversion of estuarine circulation in the Warnow estuary can occur in several ways (see shaded areas in Figure 9 for examples): (i) Inversion due to an inversed buoyancy gradient resulting from varying coastal waters. This turned out to be here the most effective driver of inversed estuarine circulation. The strength of this exchange flow is modified by along-estuary winds. (ii) Inversion due to up-estuary wind straining resulting from a relative high sensitivity of the estuary to wind forcing. This happened occasionally on the time scale of a few hours and when the buoyancy gradient forcing is weak, for example, larger local Wedderburn numbers. (iii) Inversion of the inversed circulation resulting in a classical exchange. The latter is the case when down-estuary wind forcing drives a positive circulation even though the buoyancy gradient is reversed. This complex interaction of gravitational circulation and wind forcing, both with varying signs, is found to result in three-layered velocity profiles (Figure 9d).

When considering long-term averages of inflow and outflow salinity, resulting from the exchange flow and mixing in the estuary, it turns out that they change proportionally with increasing inflow salinity causing an increase in the outflow salinity. The proportionality factor of 84% suggests that the outflowing water consists to 84% of recirculated seawater and 16% of freshwater discharge. Recent salinity mixing theories by MacCready et al. (2018) and Burchard et al. (2019) suggest that this factor additionally represents the mixing completeness (ratio of actual mixing to maximum possible mixing) of the estuary, connecting estuarine-wide mixing information with salinity values at the mouth. The mixing completeness of $M_C = 84\%$ is larger than values calculated by Burchard et al. (2019) for the Baltic Sea ($Mc = 54\%$). Making use of an idealized estuary with tidal forcing, MacCready et al. (2018) recently showed that the mixing completeness in their study varied between 95% and 62% during spring and neap tide, respectively. As pointed out by MacCready et al. (2018), more estuaries have to be studied in terms of this new mixing approach in order to put these numbers into context.

However, the results show that the volume-integrated mixing, the volume-averaged salinity, and the volume-integrated salinity variance are highly variable over time. The comparison of the volume-integrated mixing (i) obtained by the numerical model and (ii) calculated using the simple relation $M \approx s_{\mathrm{in}} s_{\mathrm{out}} Q_r$ proposed by MacCready et al. (2018) shows largely good agreement. Deviations between the exact and the analytically calculated mixing can be explained by the fact that the simple analytical formulation neglects inflow and outflow fluxes of s^2 as identified by Burchard et al. (2019). When calculating the mixing timescale as the ratio of the total salinity variance to the total mixing, the results for the Warnow estuary are in the order of 1 day but increase if the total mixing decreases. A possible reason for the decreased mixing during certain events is an already vertically homogenized water column as indicated by small values of the volume-integrated potential energy anomaly. The latter coincides with increased values of surface stress, suggesting that the estuary is mixed vertically due to wind and thus decreased in stratification, while still existing horizontal density gradients result in spatial salinity variance.

5. Conclusions

The Warnow estuary is exposed to volatile along-estuary wind forcing as well as strong variations in salinity, due to its location between the high saline North Sea and the brackish water of the Baltic Sea. The exchange flow changes between classical and inversed circulation, which is described in a parameter space spanned by the Simpson number Si and the non-dimensional wind stress Ts. The basic Wedderburn number of $\mathrm{We}_b \approx 30\%$ for cancellation of gravitational forcing by wind forcing could be confirmed as a promising parameter for comparisons between different estuaries with respect to their sensitivity to wind stress, since We_b is found to be largely independent of the state of the estuary. The results underline the importance of the orientation of the estuary with respect to the prevailing wind directions. Using the framework of the TEF, recent formulations for the volume-integrated mixing and the mixing completeness showed their robustness when applied to a volatile system. The newly introduced mixing time scale T_{mix} can extend the set of bulk parameters for understanding mixing processes in estuaries.

Unanswered is the question which non-dimensional parameter may describe the dynamics driven by gravitational forcing in weakly tidal estuaries, since the Simpson number turns out to be unusually large as a consequence of small bottom friction velocities. A promising candidate might be the reciprocal Wedderburn number $1/\mathrm{We} = \mathrm{Si}/\mathrm{Ts} = \partial_x b H^2 / u_*^s |u_*^s| = \mathrm{Si}^*$ which may be interpreted as a modified Simpson number using the surface friction velocity scale. Investigating additional estuaries would be helpful in setting the mixing completeness in a broader context, which is also true for the basic Wedderburn number and the estuarine mixing time scale T_{mix}. The latter raises the question whether time values of 1 day, as found for the Warnow estuary, are typical of certain types of estuaries.

Data Availability Statement

The data analysis was performed by computers financed by PROSO (FKZ: 03F0779A), and the data underlying this study are available online (at https://thredds-iow.io-warnemuende.de/thredds/catalogs/regions/baltic/regions/catalog_jgr2020_xlange.html).

Acknowledgments

We thank the Federal Maritime and Hydrographic Agency Hamburg and Rostock (BSH) for financing and for supporting the operation of the MARNET station Darss Sill. The numerical simulations have been carried out on supercomputers of the North-German Supercomputing Alliance (HLRN). This study was funded by the Deutsche Forschungsgemeinschaft (DFG) project BalticTRANSCOAST under Grant GRK 2000/1 and the BMBF project MicroCatch_Balt (03F0788A). Open access funding enabled and organized by Projekt DEAL.

References

Barsi, J. A., Barker, J. L., & Schott, J. R. (2003). An atmospheric correction parameter calculator for a single thermal band earth-sensing instrument. *IEEE International Geoscience and Remote Sensing Symposium 2003*, *5*, 2–4.

Becherer, J., Stacey, M. T., Umlauf, L., & Burchard, H. (2015). Lateral circulation generates flood tide stratification and estuarine exchange flow in a curved tidal inlet. *Journal of Physical Oceanography*, *45*, 638–656. https://doi.org/10.1175/JPO-D-14-0001.1

Burchard, H., & Bolding, K. (2002). Three-dimensional modelling of estuarine turbidity maxima in a tidal estuary: European Commission.

Burchard, H., Bolding, K., Feistel, R., Gräwe, U., Klingbeil, K., MacCready, P., et al. (2018). The Knudsen theorem and the Total Exchange Flow analysis framework applied to the Baltic Sea. *Progress in Oceanography*, *165*, 268–286. https://doi.org/10.1016/j.pocean.2018.04.004

Burchard, H., Bolding, K., & Villarreal, M. R. (1999). GOTM, a general ocean turbulence model. Theory, implementation and test cases: European Comission.

Burchard, H., Hetland, R. D., Schulz, E., & Schuttelaars, H. M. (2011). Drivers of residual estuarine circulation in tidally energetic estuaries: Straight and irrotational channels with parabolic cross section. *Journal of Physical Oceanography*, *41*, 548–570. https://doi.org/10.1175/2010JPO4453.1

Burchard, H., & Hofmeister, R. (2008). A dynamic equation for the potential energy anomaly for analysing mixing and stratification in estuaries and coastal seas. *Estuarine, Coastal and Shelf Science*, *77*, 679–687.

Burchard, H., Janssen, F., Bolding, K., Umlauf, L., & Rennau, H. (2009). Model simulations of dense bottom currents in the Western Baltic Sea. *Continental Shelf Research*, *29*, 205–220. https://doi.org/10.1016/j.csr.2007.09.010

Burchard, H., Lange, X., Klingbeil, K., & MacCready, P. (2019). Mixing estimates for estuaries. *Journal of Physical Oceanography*, *49*, 631–648. https://doi.org/10.1175/jpo-d-18-0147.1

Burchard, H., & Rennau, H. (2008). Comparative quantification of physically and numerically induced mixing in ocean models. *Ocean Modelling*, *20*, 293–311.

Burchard, H., Schulz, E., & Schuttelaars, H. M. (2014). Impact of estuarine convergence on residual circulation in tidally energetic estuaries and inlets. *Geophysical Research Letters*, *41*, 913–919. https://doi.org/10.1002/2013GL058494

Chant, R. J. (2002). Secondary circulation in a region of flow curvature: Relationship with tidal forcing and river discharge. *Journal of Geophysical Research*, *107*(C9), 3131. https://doi.org/10.1029/2001JC001082

Chatwin, P. C. (1976). Some remarks on the maintenance of the salinity distribution in estuaries. *Estuarine and Coastal Marine Science*, *4*, 555–566. https://doi.org/10.1016/0302-3524(76)90030-X

Chen, S.-N., & Sanford, L. P. (2009). Axial wind effects on stratification and longitudinal salt transport in an idealized, partially mixed estuary. *Journal of Physical Oceanography*, *39*, 1905–1920. https://doi.org/10.1175/2009JPO4016.1

Flöser, G., Burchard, H., & Riethmller, R. (2011). Observational evidence for estuarine circulation in the German Wadden Sea. *Continental Shelf Research*, *31*, 1633–1639.

Geyer, W. R. (1993). Three-dimensional tidal flow around headlands. *Journal of Geophysical Research*, *98*, 955–966. https://doi.org/10.1029/92JC02270

Geyer, W. R., & MacCready, P. (2014). The estuarine circulation. *Annual Review of Fluid Mechanics*, *46*, 175–197. https://doi.org/10.1146/annurev-fluid-010313-141302

Geyer, W. R., & Ralston, D. K. (2015). Estuarine frontogenesis. *Journal of Physical Oceanography*, *45*, 546–561.

Gräwe, U., Flöser, G., Gerkema, T., Duran-Matute, M., Badewien, T. H., Schulz, E., & Burchard, H. (2016). A numerical model for the entire Wadden Sea: Skill assessment and analysis of hydrodynamics. *Journal of Geophysical Research: Oceans*, *121*, 5231–5251. https://doi.org/10.1002/2016JC011655

Gräwe, U., Holtermann, P., Klingbeil, K., & Burchard, H. (2015). Advantages of vertically adaptive coordinates in numerical models of stratified shelf seas. *Ocean Modelling*, *92*, 56–68. https://doi.org/10.1016/j.ocemod.2015.05.008

Gräwe, U., Naumann, M., Mohrholz, V., & Burchard, H. (2015). Anatomizing one of the largest saltwater inflows into the Baltic Sea in December 2014. *Journal of Geophysical Research: Oceans*, *120*, 7676–7697. https://doi.org/10.1002/2015JC011269

Gräwe, U., & Wolff, J.-O. (2010). Suspended particulate matter dynamics in a particle framework. *Environmental Fluid Mechanics*, *10*, 21–39.

Hansen, D. V., & Rattray, M. (1965). Gravitational circulation in straits and estuaries. *Journal of Marine Research*, *23*, 104–122. https://doi.org/10.1098/rspb.2009.2214

Hetland, R. D., & Geyer, W. R. (2004). An idealized study of the structure of long, partially mixed estuaries. *Journal of Physical Oceanography*, *34*, 2677–2691. https://doi.org/10.1175/JPO2646.1

Hofmeister, R., Burchard, H., & Beckers, J.-M. (2010). Non-uniform adaptive vertical grids for 3D numerical ocean models. *Ocean Modelling*, *33*, 70–86.

Holtermann, P. L., Burchard, H., Gräwe, U., Klingbeil, K., & Umlauf, L. (2014). Deep-water dynamics and boundary mixing in a nontidal stratified basin: A modeling study of the Baltic Sea. *Journal of Geophysical Research: Oceans*, *119*, 1465–1487. https://doi.org/10.1002/2013JC009483

Ianniello, J. P. (1979). Tidally induced residual currents in estuaries of variable breadth and depth. *Journal of Physical Oceanography*, *9*, 962–974.

Johns, W. E., Yao, F., Olson, D. B., Josey, S. A., Grist, J. P., & Smeed, D. A. (2003). Observations of seasonal exchange through the Straits of Hormuz and the inferred heat and freshwater budgets of the Persian Gulf. *Journal of Geophysical Research*, *108*, 3391. https://doi.org/10.1029/2003JC001881

Klingbeil, K., Becherer, J., Schulz, E., de Swart, H. E., Schuttelaars, H. M., Valle-Levinson, A., & Burchard, H. (2019). Thickness-weighted averaging in tidal estuaries and the vertical distribution of the Eulerian residual transport. *Journal of Physical Oceanography*, *49*, 1809–1826. https://doi.org/10.1175/JPO-D-18-0083.1

Klingbeil, K., & Burchard, H. (2013). Implementation of a direct nonhydrostatic pressure gradient discretisation into a layered ocean model. *Ocean Modelling*, *65*, 64–77. https://doi.org/10.1016/j.ocemod.2013.02.002

Klingbeil, K., Lemarié, F., Debreu, L., & Burchard, H. (2018). The numerics of hydrostatic structured-grid coastal ocean models: State of the art and future perspectives. *Ocean Modelling*, *125*, 80–105.

Klingbeil, K., Mohammadi-Aragh, M., Gräwe, U., & Burchard, H. (2014). Quantification of spurious dissipation and mixing—Discrete variance decay in a finite-volume framework. *Ocean Modelling*, *81*, 49–64. https://doi.org/10.1016/j.ocemod.2014.06.001

Knudsen, M. (1900). Ein hydrographischer Lehrsatz. *Hydrographie und Maritimen Meteorologie*, *28*, 316–320.

Lange, X., & Burchard, H. (2019). The relative importance of wind straining and gravitational forcing in driving exchange flows in tidally energetic estuaries. *Journal of Physical Oceanography*, *49*, 723–736. https://doi.org/10.1175/jpo-d-18-0014.1

Lorenz, M., Klingbeil, K., MacCready, P., & Burchard, H. (2019). Numerical issues of the Total Exchange Flow (TEF) analysis framework for quantifying estuarine circulation. *Ocean Science*, *15*, 601–614. https://doi.org/10.5194/os-15-601-2019

MacCready, P. (2011). Calculating estuarine exchange flow using isohaline coordinates. *Journal of Physical Oceanography*, *41*, 1116–1124. https://doi.org/10.1175/2011JPO4517.1

MacCready, P., & Geyer, W. R. (2010). Advances in estuarine physics. *Annual Review of Marine Science*, *2*, 35–58. https://doi.org/10.1146/annurev-marine-120308-081015

MacCready, P., Geyer, W. R., & Burchard, H. (2018). Estuarine exchange flow is related to mixing through the salinity variance budget. *Journal of Physical Oceanography*, *48*, 1375–1384. https://doi.org/10.1175/JPO-D-17-0266.1

Matthäus, W., & Schinke, H. (1999). The influence of river runoff on deep water conditions of the Baltic Sea. *Hydrobiologia*, *393*, 1–10.

Nunes, R. A., & Lennon, G. W. (1986). Physical property distributions and seasonal trends in Spencer Gulf, South Australia: An inverse estuary. *Australian Journal of Marine and Freshwater Research*, *37*, 39–53.

Pritchard, D. W. (1952). Salinity distribution and circulation in the Chesapeake Bay estuarine system. *Journal of Marine Research*, *11*, 106–123.

Pritchard, D. W. (1954). A study of the salt balance in a coastal plain estuary. *Journal of Marine Research*, *13*, 133–144.

Pritchard, D. W. (1956). The dynamic structure of a coastal plain estuary. *Journal of Marine Research*, *15*, 33–42.

Purkiani, K., Becherer, J., Klingbeil, K., & Burchard, H. (2016). Wind-induced variability of estuarine circulation in a tidally energetic inlet with curvature. *Journal of Geophysical Research*, *121*, 3261–3277. https://doi.org/10.1002/2015JC010945

Sassi, M. G., Duran-Matute, M., van Kessel, T., & Gerkema, T. (2015). Variability of residual fluxes of suspended sediment in a multiple-inlet system: The Dutch Wadden Sea. *Ocean Dynamics*, *65*, 1321–1333. https://doi.org/10.1007/s10236-015-0866-2

Schiele, K. S., Darr, A., Zettlr, M. L., Friedland, R., Tauber, F., Weber, M., & Voss, J. (2015). Biotope map of the German Baltic Sea. *Marine Pollution Bulletin*, *96*, 127–135.

Schulz, E., Schuttelaars, H. M., Gräwe, U., & Burchard, H. (2015). Impact of the depth-to-width ratio of periodically stratified tidal channels on the estuarine circulation. *Journal of Physical Oceanography*, *45*, 2048–2069.

Scully, M. E., Friedrichs, C., & Brubaker, J. (2005). Control of estuarine stratification and mixing by wind-induced straining of the estuarine density field. *Estuaries*, *28*, 321–326. https://doi.org/10.1007/BF02693915

Simpson, J. H. (1981). The shelf-sea fronts: Implications of their existence and behaviour. *Philosophical Transactions of the Royal Society of London. Series A*, *302*, 531–546.

Simpson, J. H., Brown, J., Matthews, J., & Allen, G. (1990). Tidal straining, density currents, and stirring in the control of estuarine stratification. *Estuaries*, *13*, 125–132. https://doi.org/10.2307/1351581

Stacey, M. T., Brennan, M. L., Burau, J. R., & Monismith, S. G. (2010). The tidally averaged momentum balance in a partially and periodically stratified estuary. *Journal of Physical Oceanography*, *40*, 2418–2434.

Umlauf, L., & Burchard, H. (2005). Second-order turbulence closure models for geophysical boundary layers. A review of recent work. *Continental Shelf Research*, *25*, 795–827. https://doi.org/10.1016/j.csr.2004.08.004

Wang, T., Geyer, W. R., & MacCready, P. (2017). Total exchange flow, entrainment, and diffusive salt flux in estuaries. *Journal of Physical Oceanography*, *47*, 1205–1220. https://doi.org/10.1175/JPO-D-16-0258.1